# DISCRETE ELEMENT MODELLING OF HIGHLY CRUSHABLE PUMICE SAND


**Sam Bahmani**

*Supervisors:*

**Prof Rolando Orense**

**Prof Michael Pender**

# Outline

- Introduction
- Literature review
- Problem statement
- Objectives
- Particle crushing criteria
- Results
- Conclusions

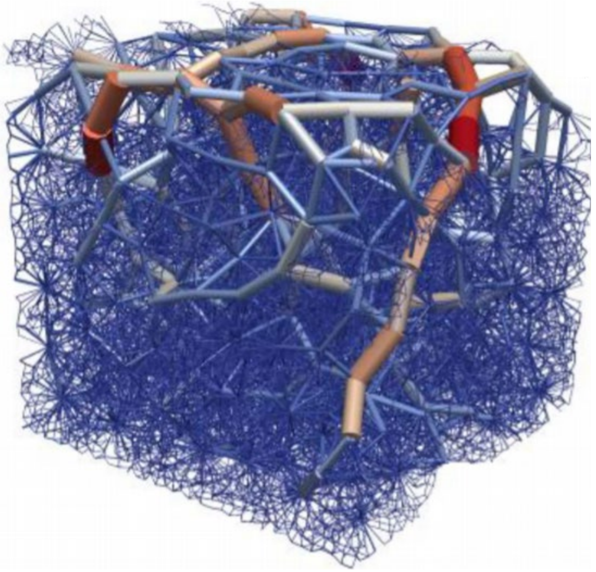

# Introduction

- problematic from engineering perspective:

  - **Vesicular nature**

    (Internal and surface voids)

  - **Unique surface texture**

  → 
  - Crushable
  - Compressible
  - Lightweight

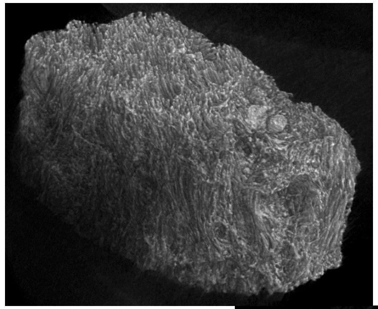

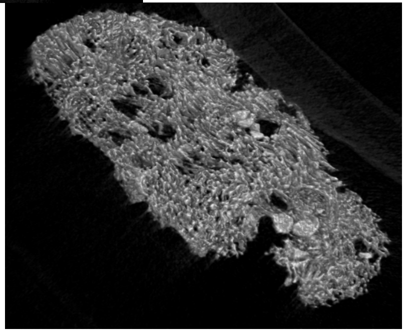

- The information currently available on the geotechnical characteristics of pumice sands is limited.

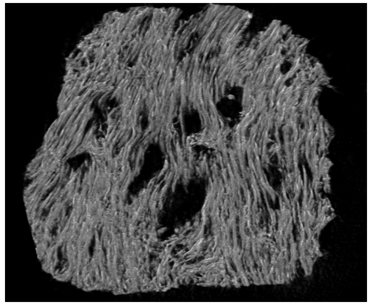

- Attributed to the time-consuming and expensive nature of laboratory testing, implemented to characterise its behaviour.

# Problem statement

- Lack of information on pumice sands for required DEM parameters;
- A DEM model, with consideration of the crushing response based on the experimental results and irregular shape of the particles under various conditions for pumice sand.
- Developing an efficient model to account for implementing the particle crushing mechanism and impact of crushing on the other particles in the sand matrix;
- Effects of boundary condition, drainage condition, shape of particles, void ratio, and different loading impact such as cyclic loading.

# Objectives

- Influence of the shape and crushability on the behaviour of pumice sands;
- Calibrated DEM results with the results of laboratory experiments;
- Accurately predict the response of pumice sand particles;
- Better understanding of the behaviour of pumice sands subjected to loading conditions;
- Micromechanical behaviour of pumice sands at the microscale and macroscale level.

# Results

## 3D scanning

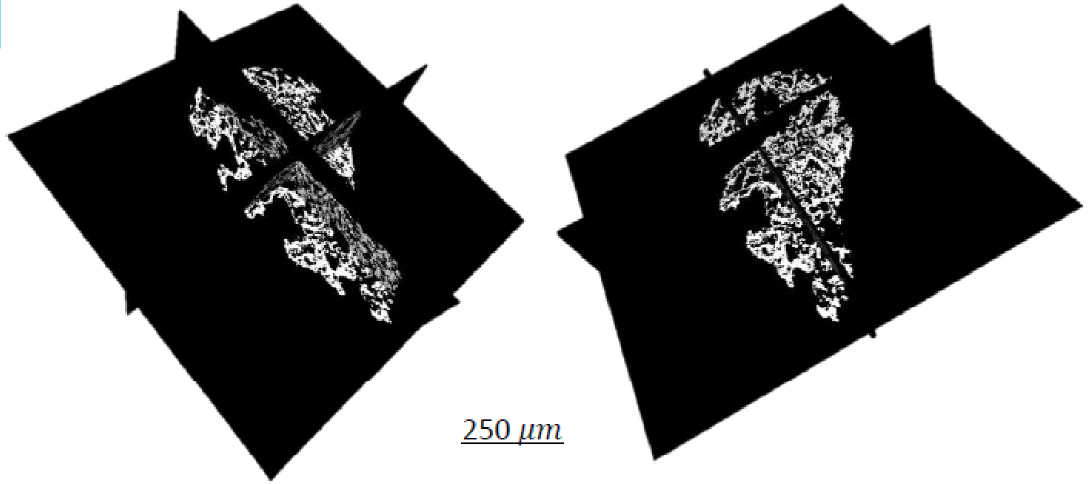


| | |
|---|---|
| Specific gravity, $G_s$ | 1.7 - 2.3 |
| Maximum void ratio, $e_{\max}$ | 2.0 - 2.5 |
| Minimum void ratio, $e_{\min}$ | 1.1 - 1.7 |
| Particle size, mm | 0.5 – 2.5 |

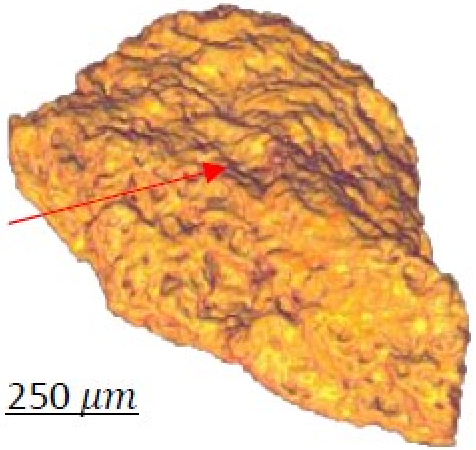


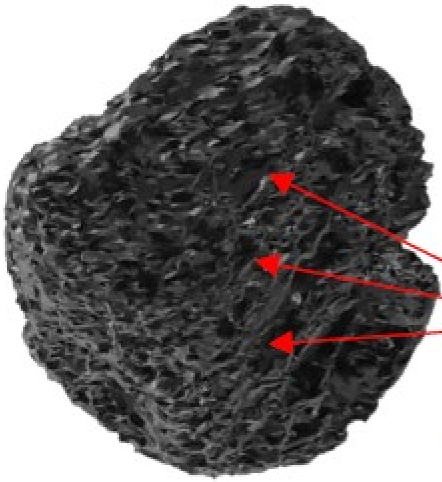

# Results (cont.)

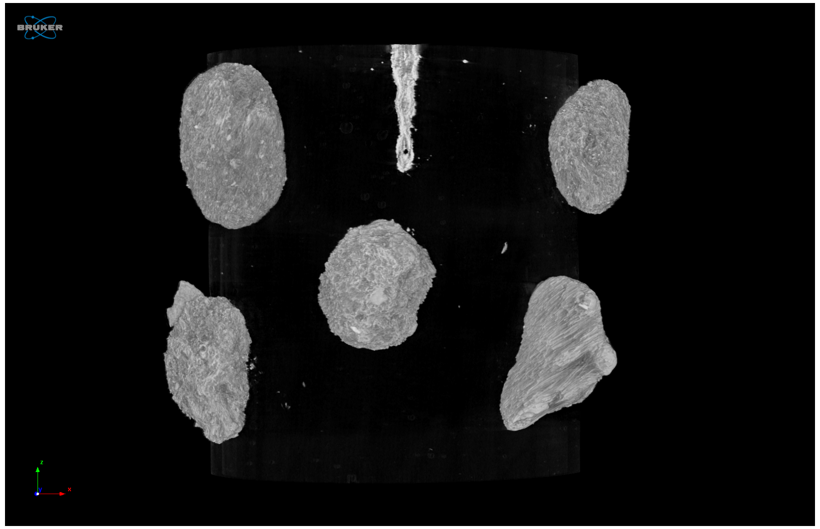

Table 1. Scan parameters employed for the µX-CT scanner and cross-sectional reconstruction.

| µX-CT parameters | | Reconstruction parameters | |
|---|---|---|---|
| Pixel size (µm) | 2.5 | Artifact correction | 12 |
| X-ray voltage (kV) | 60 | Beam hardening correction (%) | 64 |
| X-ray current (µA) | 166 | Smoothing | 1 |
| Rotation step (°) | 0.30 | Static rotation | 0.0 |
| Filter | All | Cone-beam angle vertical | 12 |
| Frame averaging | Off | Cone-beam angle horizontal | 8 |

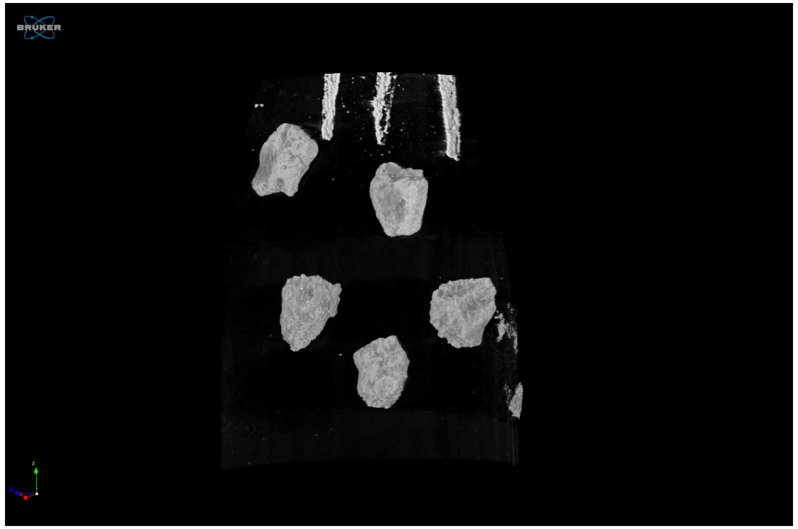

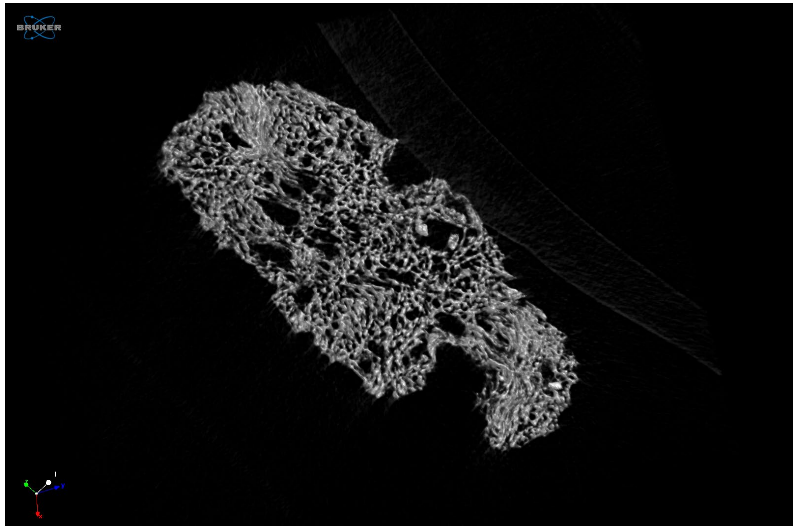

# 3D scanning analysis

| Closed porosity (percent) | Volume of open pore space | Open porosity (percent) | Total volume of pore space | Total porosity (percent) |
|---|---|---|---|---|
| Po(cl) | Po.V(op) | Po(op) | Po.V(tot) | Po(tot) |
| % | U^3 | % | U^3 | % |
| 0.07783516 | 1268774205 | 46.99998607 | 1269887828 | 47.04123871 |
| | 1.268774 mm3 | 47% | 1.269888 mm3 | |

| Name | Particle size | Open porosity (%) | |
|---|---|---|---|
| PP-1 | 2.5 | 47 | |
| PP-2 | 2.3 | 44 | |
| PP-3 | 2.2 | 43 | |
| PP-4 | 2.4 | 49 | |
| PP-5 | 1.5 | 31 | |
| PP-6 | 2.4 | 49 | |
| PP-7 | 1 | 32 | |
| PP-8 | 2 | 40 | |
| PP-9 | 1.7 | 36 | |
| PP-10 | 1.3 | 32 | |
| | Total Average | 40.3 | 40 |

| Name | Particle size | Closed porosity (%) | |
|---|---|---|---|
| PP-1 | 2.5 | 0.07 | |
| PP-2 | 2.3 | 0.05 | |
| PP-3 | 2.2 | 0.04 | |
| PP-4 | 2.4 | 0.06 | |
| PP-5 | 1.5 | 0.03 | |
| PP-6 | 2.4 | 0.06 | |
| PP-7 | 1 | 0.02 | |
| PP-8 | 2 | 0.03 | |
| PP-9 | 1.7 | 0.03 | |
| PP-10 | 1.3 | 0.02 | |
| | Total Average | 0.041 | 0.04 |

# PARTICLE STRENGT SIZE RELATION

$$\sigma = \frac{F}{h_0^2}$$

$$P_s = 1 - i/(N+1)$$

$$P_s(d) = exp\left[-\left(\frac{\sigma}{\sigma_0}\right)^m\right]$$

$$ln\left[ln\left(\frac{1}{P_s}\right)\right] = m \cdot ln\left(\frac{\sigma}{\sigma_0}\right)$$

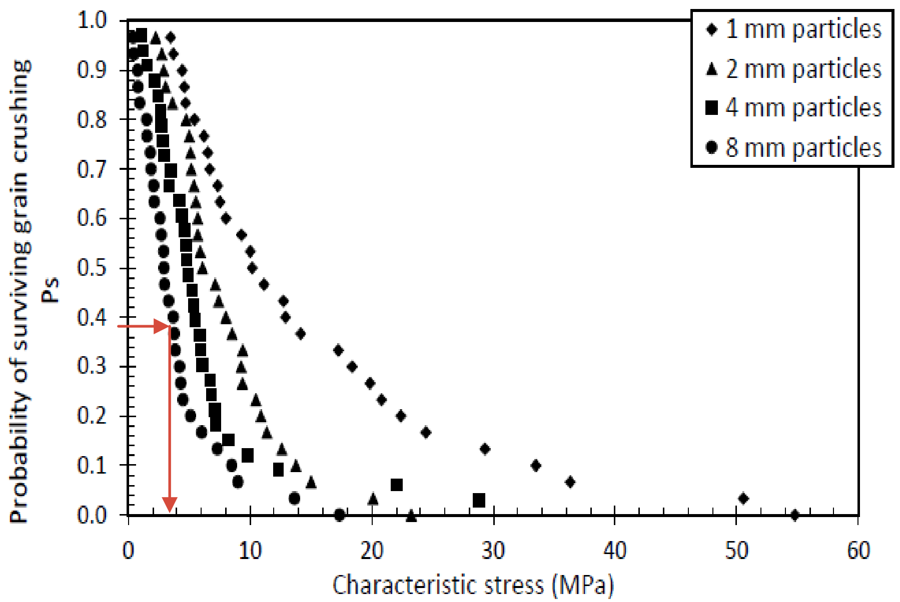


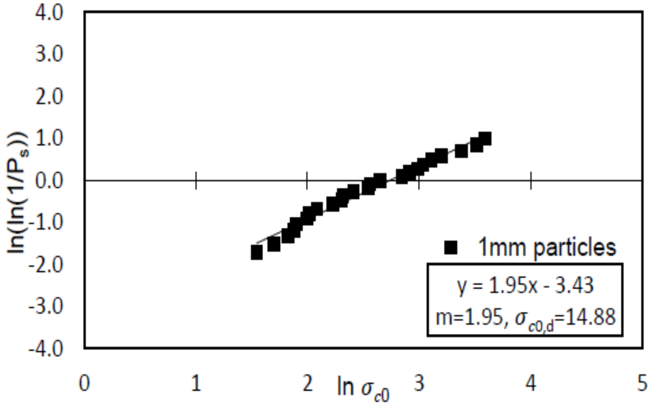


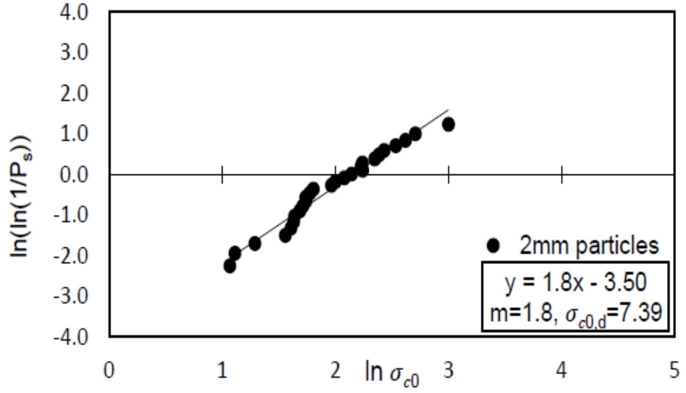

# Results (cont.)

| Nominal size (mm) | Weibull modulus m | 37% tensile strength ($\sigma_{C0,d}$-MPa) |
|---|---|---|
| 1 | 1.95 | 14.88 |
| 2 | 1.8 | 7.39 |
| 4 | 0.47 | 5.64 |
| 8 | 0.78 | 4.06 |

| Average size at failure (mm) | Average force at failure (N) | Predicted force at failure (N) |
|---|---|---|
| 1 | 10.4 | 9.13 |
| 2 | 17.36 | 19.43 |
| 4 | 48.68 | 55.53 |
| 8 | 72.22 | 77.85 |

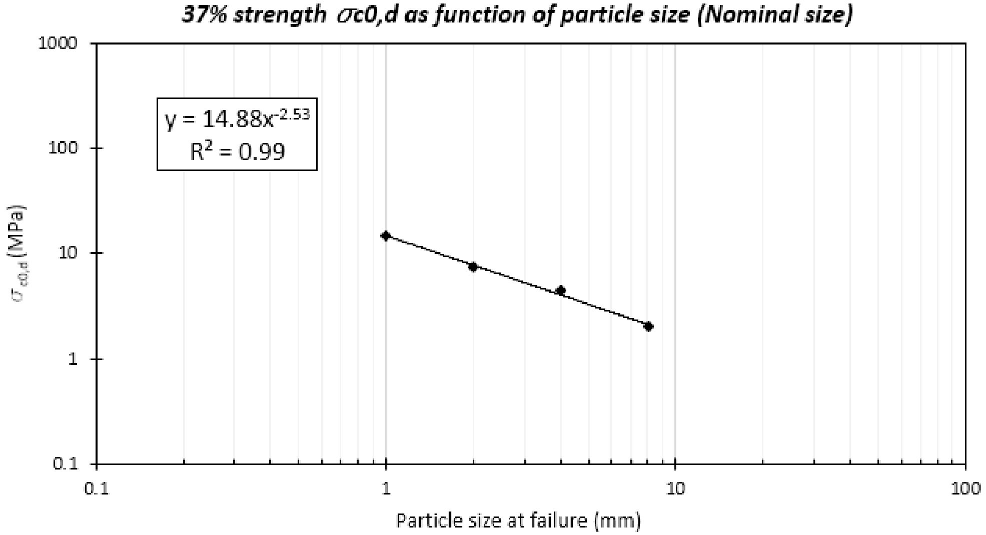


$$F_{av} \approx \sigma_{c,av} . d_{av}^2$$

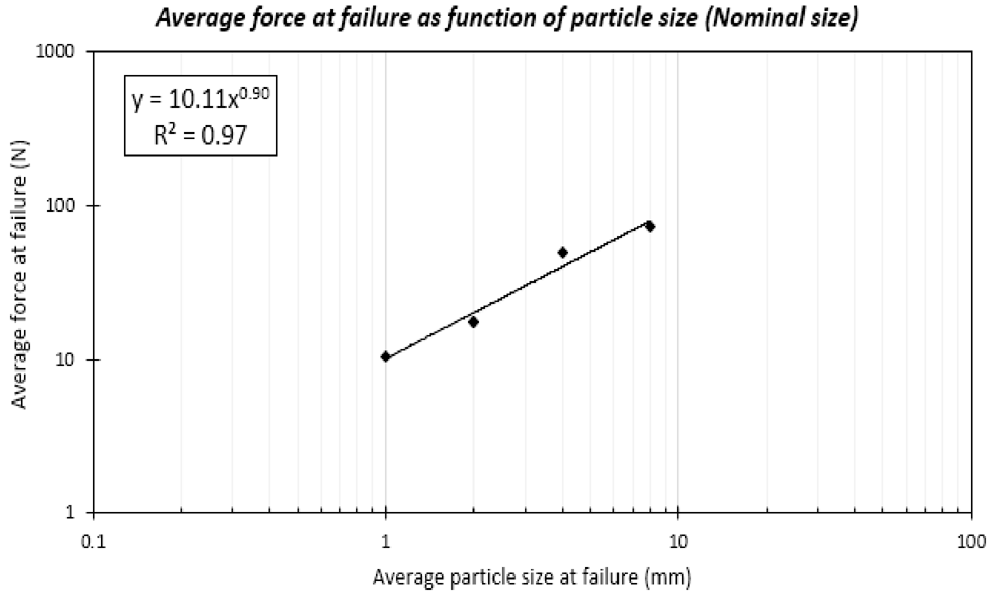


$$\sigma_{c,av} = \sigma_{co,d} \int_0^\infty x^{1/m} e^{-x} \, dx = \sigma_{co,d} \Gamma(1 + 1/m)$$

# PARTICLE CRUSHING CRITERIA

- As particle crushing criteria, a linear elastic formulation was used:

$$F = \sigma_{lim} \cdot A_F$$

$$\bar{\sigma}_{lim} = \sigma_{lim0} \cdot \left(\frac{d}{d0}\right)^{-3/m}$$

$$F \leq \left\{ \sigma_{lim0} \cdot \left(\frac{d}{d0}\right)^{-\frac{3}{m}} \pi \left[ \frac{3}{4} \frac{\left(\frac{1-v_1^2}{E_1} + \frac{1-v_2^2}{E_2}\right)}{\left(\frac{1}{r_1} + \frac{1}{r_2}\right)} \right]^{2/3} \right\}^3$$

$$F \leq \left( \sigma_{\lim,0} f(\text{var}) \left(\frac{d}{d_0}\right)^{-3/m} \times \pi \left\{ \frac{3}{4} \frac{[(1 - v_1^2)/E_1 + (1 - v_2^2)/E_2]}{[(1/r_1) + (1/r_2)]} \right\}^{2/3} \right)^3$$

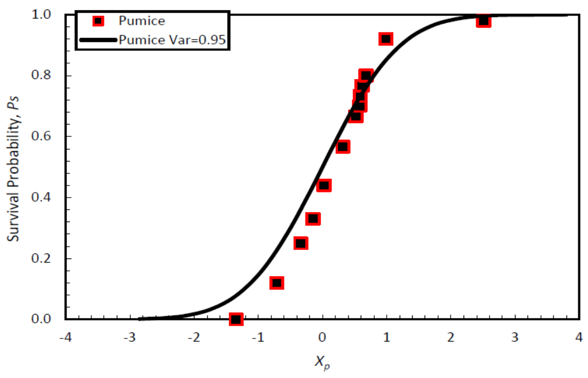


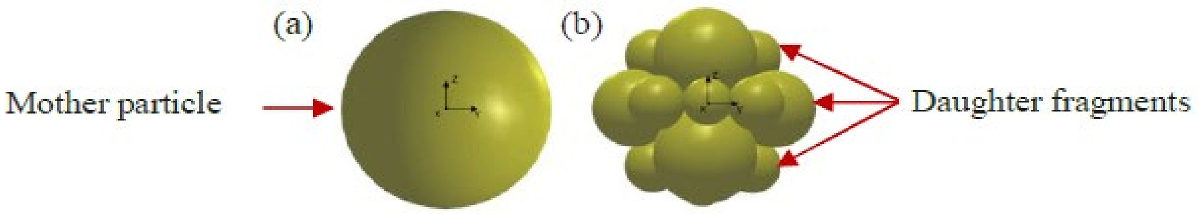


*(a) Initial particle; (b) Particle splitting configuration*

# Breakage Approaches

- Different approaches have been used to describe breakage in DEM. They can be classified in two major groups.

  I. Multigenerational approach (particle replacement)

  II. Multigrain agglomerates (Fully resolved fragments).

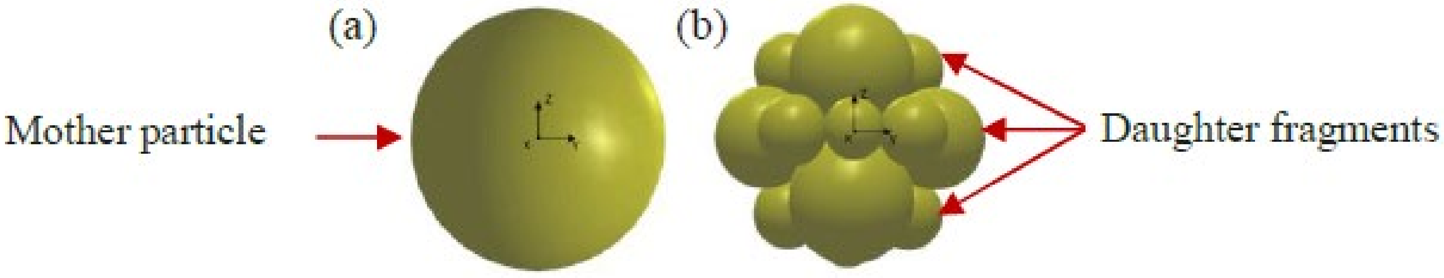


(a) Initial particle; (b) Particle splitting configuration

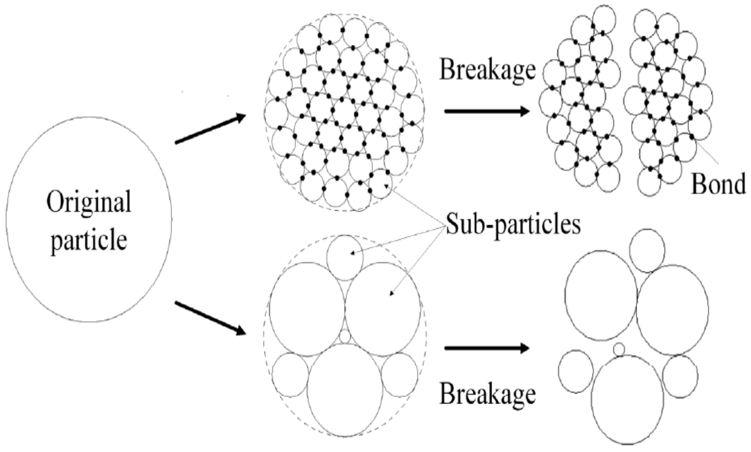

# Generation of particles

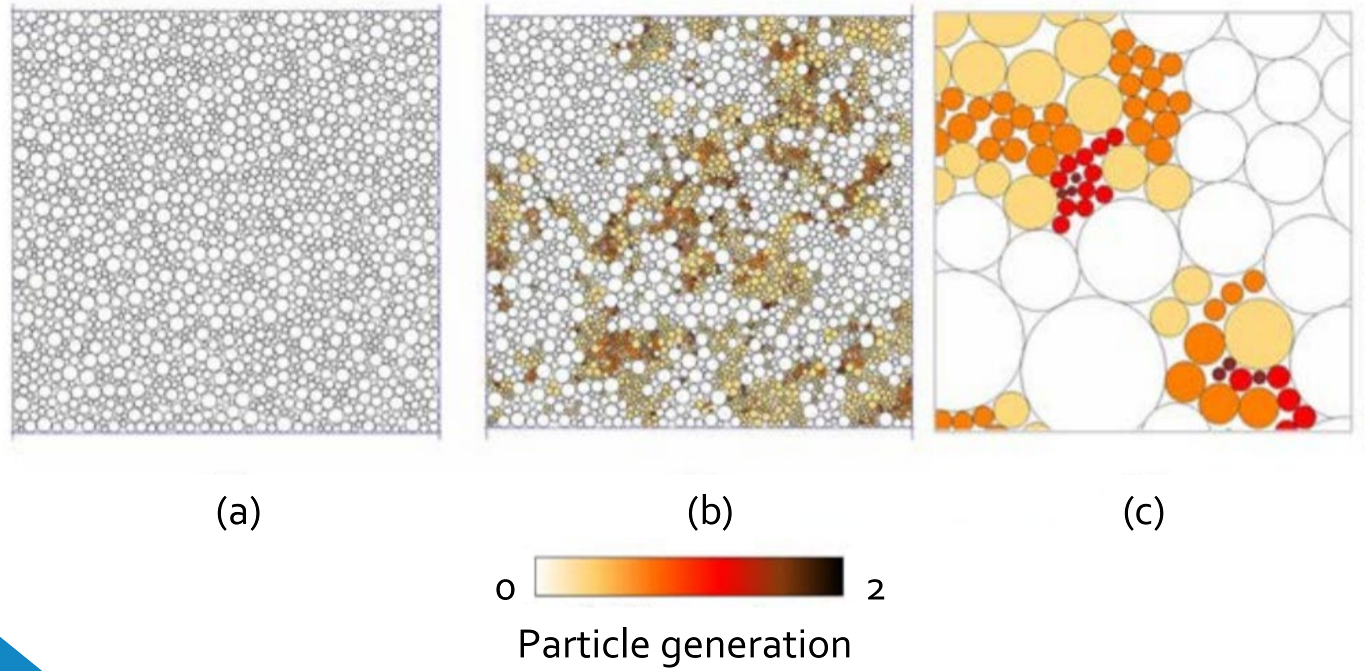


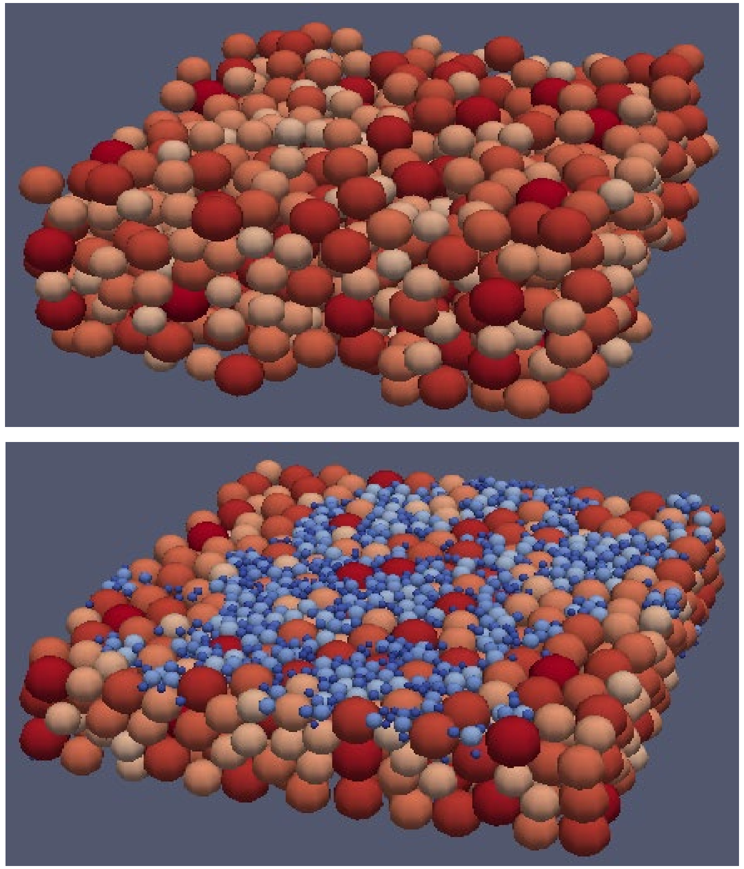

THE UNIVERSITY OF AUCKLAND
Te Whare Wananga o Tamaki Makaurau
NEW ZEALAND

# UNDRAINED TRIAXIAL

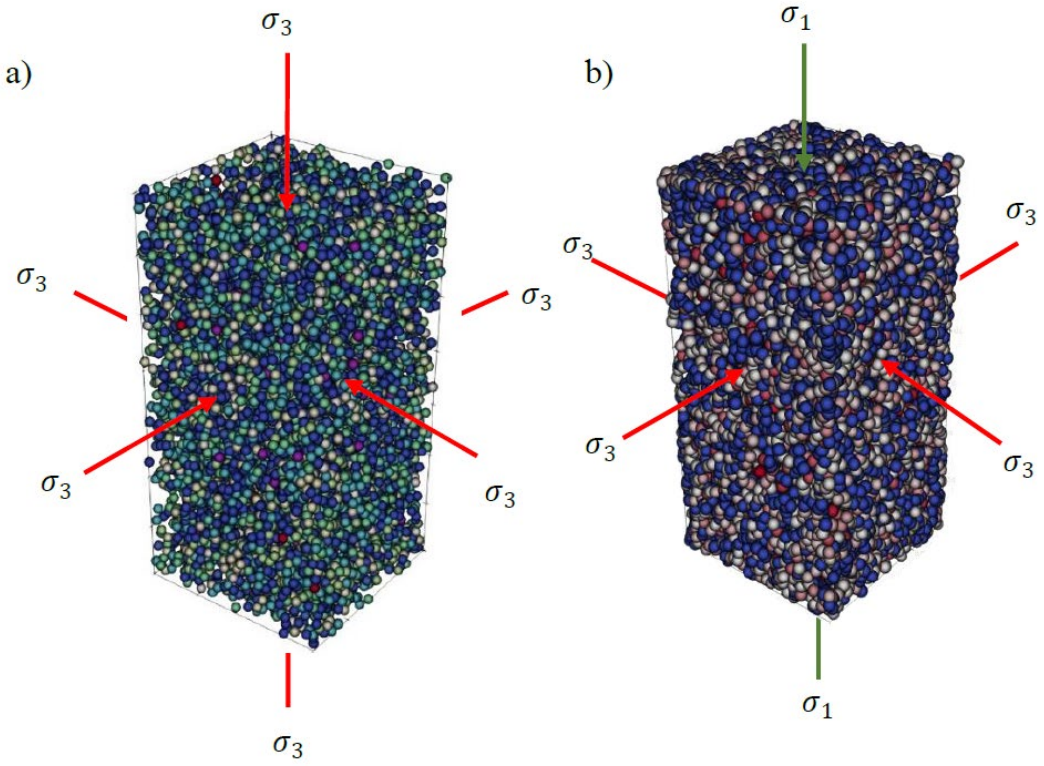


| Physical parameter | Value |
|---|---|
| Specimen dimensions ($mm^3$) | 10×10×20 |
| Number of particles | 5,000, 10,000, 20,000 |
| Friction coefficient, μ (radian) | 0.7 |
| Young's modulus, $E_0$ (MPa) | 30.1 |
| Poisson's ratio, ν | 0.25 |
| Density ($kg/m^3$) | 2000 |
| Rolling stiffness coefficient, $\beta$ | 0.125 |
| Rolling strength coefficient, $\eta$ | 0.1 |
| Friction coefficient of the wall | 0 |
| Young's modulus of the wall (GPa) | 80 |
| Poisson's ratio of the wall | 0.35 |
| Velocity (mm/s) | 0.1 |

BRIAN PERRY CIVIL

THE UNIVERSITY OF AUCKLAND
Te Whare Wananga o Tamaki Makaurau
NEW ZEALAND

# UNDRAINED TRIAXIAL

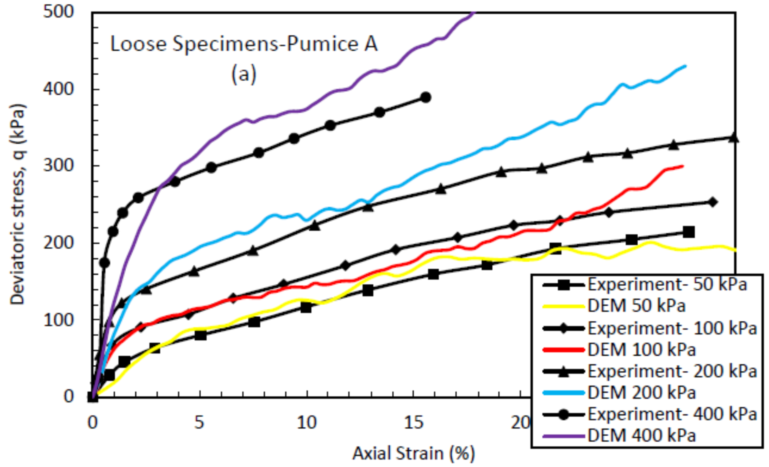


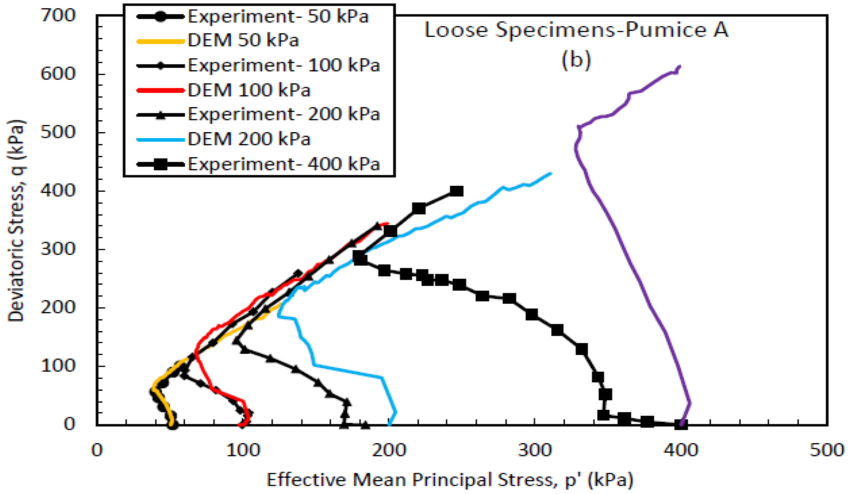


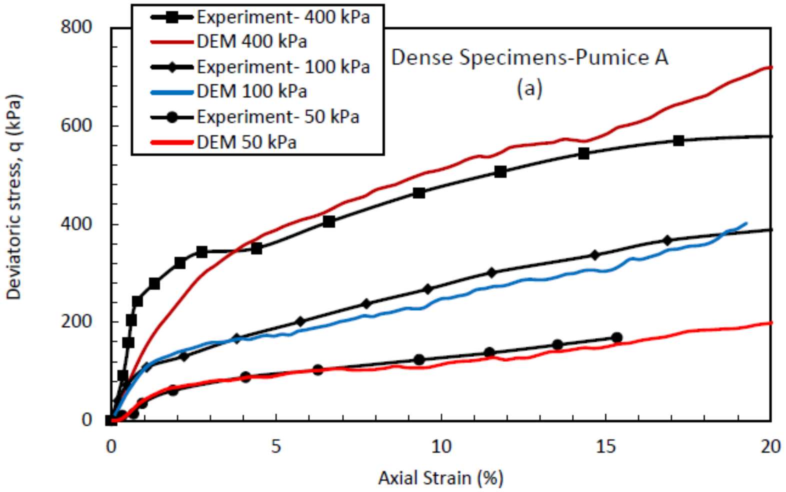


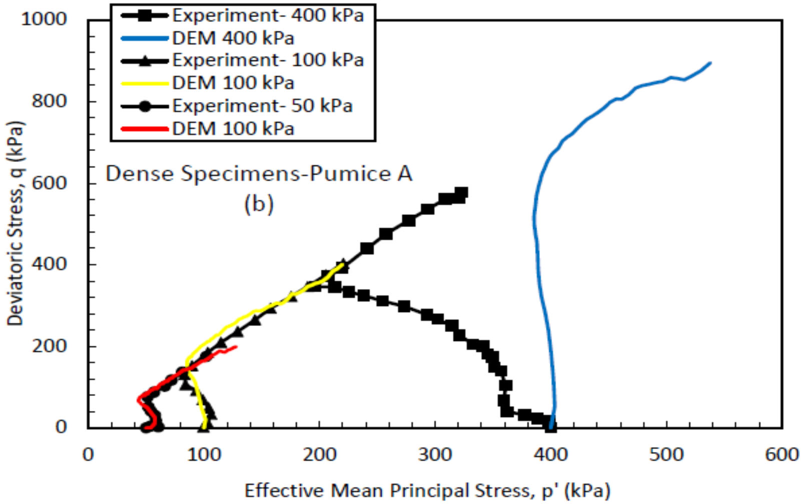

# Results (cont.)

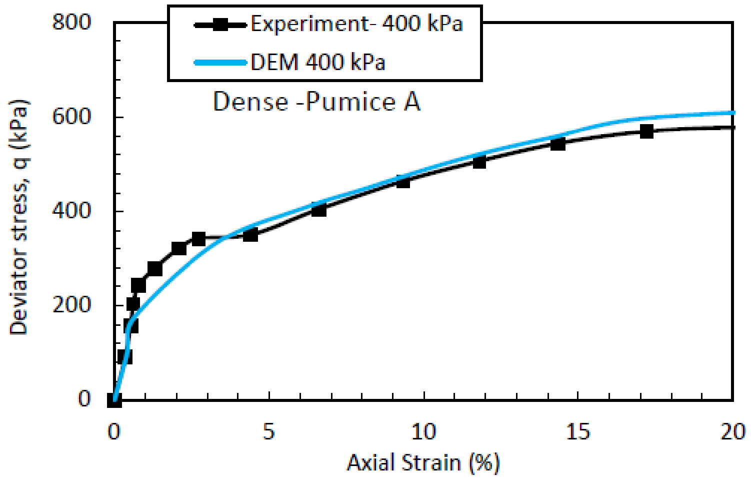


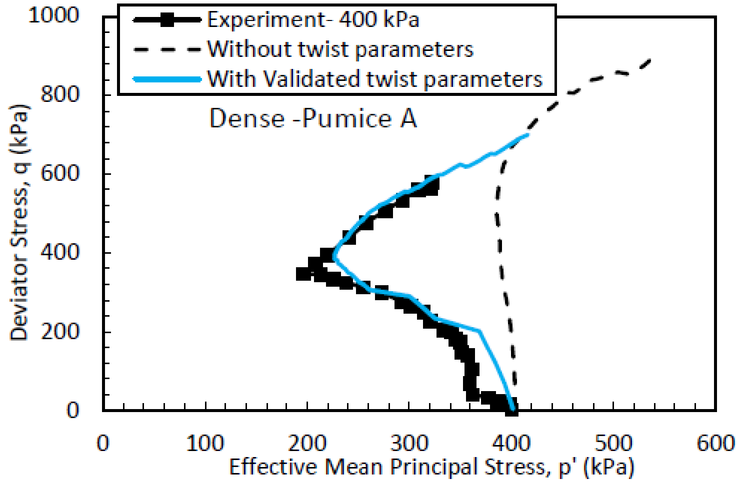


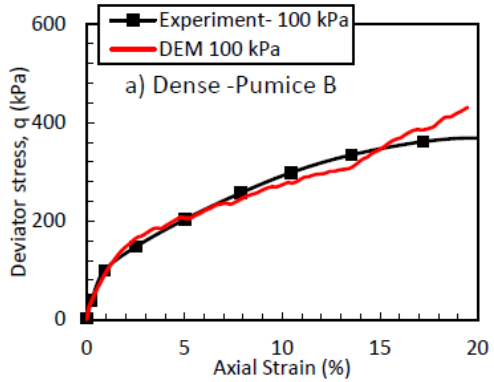


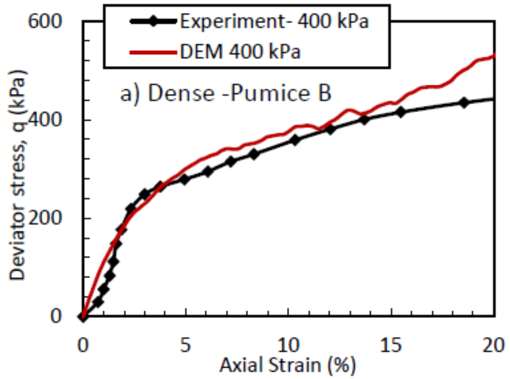


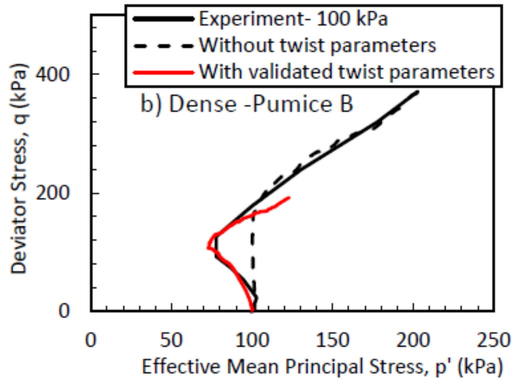


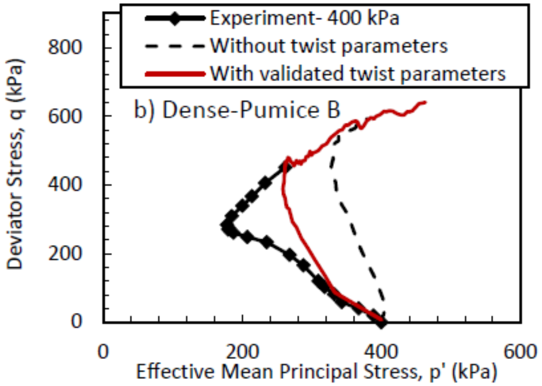


THE UNIVERSITY OF AUCKLAND
Te Whare Wananga o Tamaki Makaurau
NEW ZEALAND

BPC BRIAN PERRY CIVIL

Twist strength ($T_{wist}$); and

Twist stiffness ($K_{tw}$)

# Results (cont.)

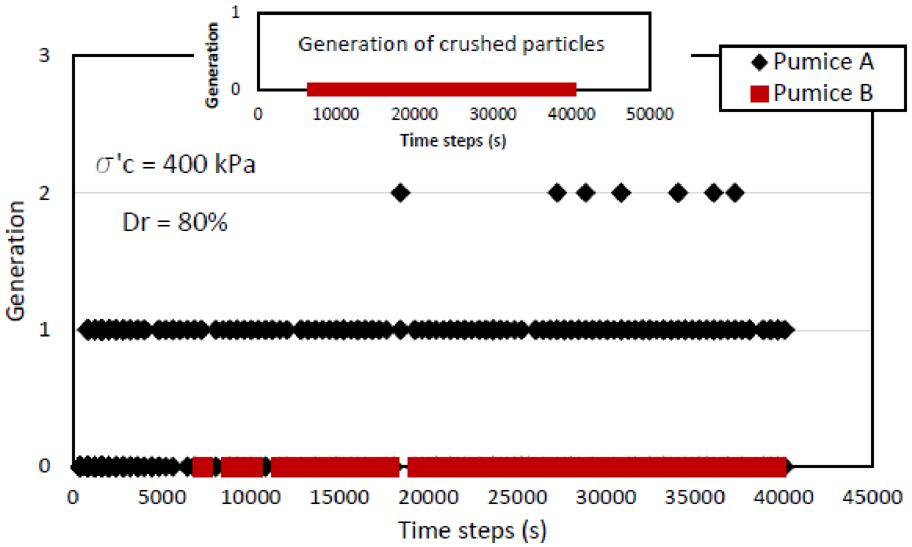


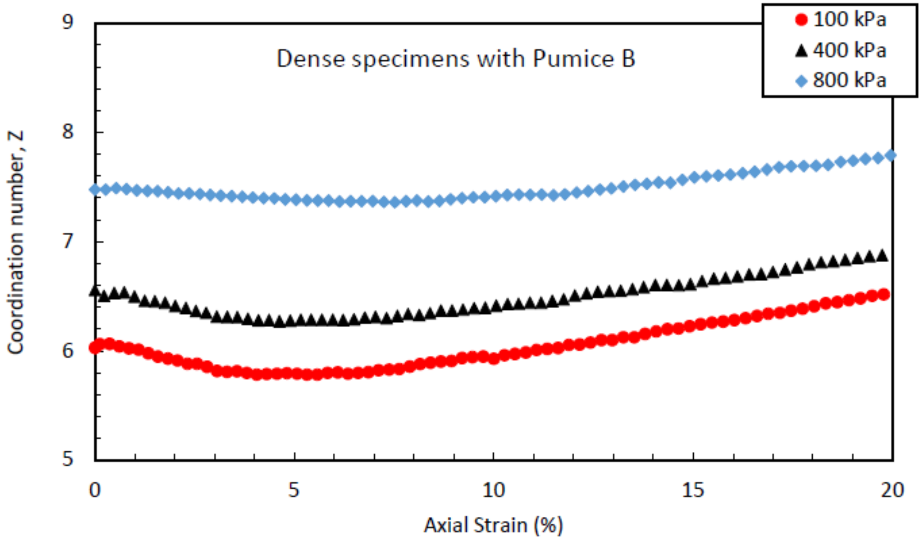


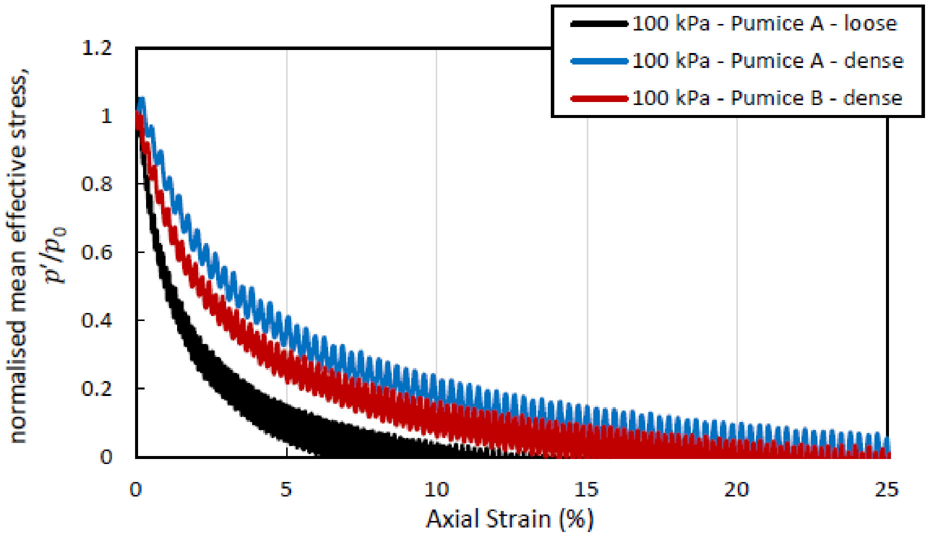


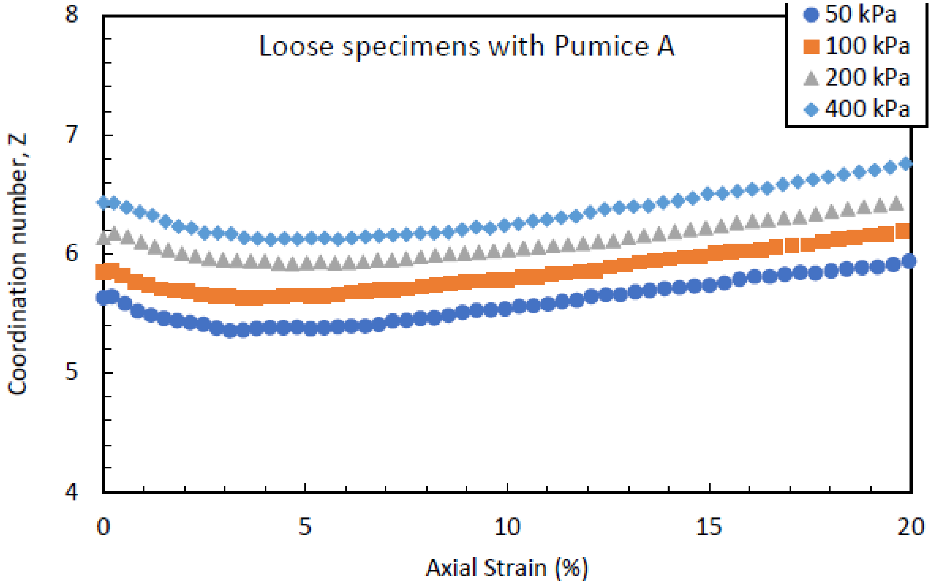

# Conclusions

- The correlation statistically showed that the crushing strength of smaller pumice particles is higher than bigger particles.

- The study also showed that the particle crushing did not stop, and particle crushing continued until the end of the tests.

- This study confirmed that the hardening behaviour of pumice specimens, not only due to the crushing, but also due to the unique surface of pumice particles.

- It was found that the limiting mechanical coordination number of corresponded to the start of the instability of the specimen.

- One of the parameters that played a key role during the simulations is the interaction between the particles, which was controlled by twisting parameters together with the rolling resistance parameters.

- The mechanical coordination Z was used to explain the instability of specimen, i.e. Z<4. The crushing phenomenon due to decreasing porosity of the specimens offered a higher resistant soil structure.

- The total number of crushed particles in dense pumice sand was roughly twice that of loose specimens. Moreover, this study proved that particle crushing occurred during the extension or unloading phase.

“Thank You”